10TH INTERNATIONAL SYMPOSIUM ON PARTICLE IMAGE VELOCIMETRY - PIV13
Delft, The Netherlands, July 1-3, 2013

Time-Resolved stereoscopic PIV measurements of cyclic variations in an internal combustion engine

Daniel-Christian Karhoff[1], Isabella Bücker[1], Michael Klaas[1], and Wolfgang Schröder[1]

[1] Chair of Fluid Mechanics and Institute of Aerodynamics, RWTH Aachen University, Aachen, Germany.
d.karhoff@aia.rwth-aachen.de

ABSTRACT

The flow field during the intake and the compression stroke of an optical four-stroke, four-valve, single-cylinder gasoline type demonstrator engine is measured using time-resolved stereoscopic particle-image velocimetry (PIV) to analyze these flow structures.

The flow is measured in the tumble plane at an engine speed of 1500 rpm in 50 consecutive cycles to account for cycle-to-cycle variations. The sampling rate is set to 3.2 kHz such that one pair of double-images is recorded at every 2.8° crank angle. Using the velocity components derived from the PIV measurements, the main vortical structure is visualized, i.e., the main tumble vortex in the symmetry plane between the inlet and outlet valves, and the temporal development of the turbulent kinetic energy is determined.

The results show high turbulent kinetic energy during the intake stroke which decreases at increasing crank angles and remains at an almost stable level during the compression stroke. At the end of compression, the vortices break up and the turbulent kinetic energy dissipates. The ensemble averaged mean kinetic energy shows that the very well conserved tumble vortex dominates the flow field during intake and compression and exhibits the typical tumble spin-up towards the end of compression, followed by a tumble break up.

A proper orthogonal decomposition of the flow field shows that the tumble vortex forms at early crank angles and dominates the flow regime, stabilizing during the compression stroke. With the beginning of the tumble breakdown, the first POD mode drops rapidly, indicating an energy transfer to higher modes.

The analysis of cyclic variations reveals significant discrepancies in the temporal development of the turbulent kinetic energy in the symmetry plane when comparing individual cycles with each other. The same applies to the path of the tumble core in the symmetry plane.

INTRODUCTION

The air-fuel mixing and hence the combustion process of piston engines is strongly influenced by the small and large scale flow structures that evolve during the intake and compression strokes [11, 12], since these turbulent flow structures interact with the flame front and influence the flame area, the propagation speed, and the stability of the flame. Generally, a high turbulence intensity during combustion is aimed for to increase the burning rate [12]. Therefore, the characterization of fuels concerning their suitability for efficient combustion processes requires not only knowledge of the chemical and combustion properties of the fuel, but also a detailed knowledge of the flow field and the fluid mechanical properties of the air-fuel mixture prior to ignition.

Huang et al. [13] investigated the relation between the flow structures and the torque and power output as well as the specific fuel consumption of an internal combustion engine. The flow field in the symmetry plane and one parallel offset plane of an optical motored engine was measured using monoscopic PIV for two inlet port configurations. Additionally, the same engine geometry was used for a fired engine to measure performance data. The measurements showed that the elliptic inlet port generates higher tumble ratios and turbulent intensities in comparison to the circular intake port. The fired experiments revealed that the higher turbulence intensity and higher tumble ratio result in a higher power output and a lower specific fuel consumption. The results evidenced the close relationship of flow condition, i.e., vortical flow and the relating mixing processes, and combustion efficiency.

Although PIV measurements of in-cylinder flow have been conducted for more than 20 years [16], stereoscopic (3C) PIV measurements of in-cylinder flows are hardly discussed in the literature. To the authors' knowledge, it has been applied only by Calendini et al. [5] and Bücker et al. [3]. In the latter study, the cycle-averaged temporal evolution of the flow field was analyzed by stereoscopic PIV measurements at 15 crank angles during intake and compression stroke in 14 axial planes, thus covering almost the entire combustion chamber. The measurements revealed a clockwise moving tumble vortex, whose core has a c-shape at first and which straightens out at the end of the compression. The mean kinetic energy is conserved until late compression by the tumble motion. This conservation provides an enhanced air motion which is beneficial for the mixing process and thus, for the combustion.

One of the major challenges in modern engine design is the understanding of cyclic variations [1]. Cyclic variations are variations in the in-cylinder flow field during induction and compression which impact the mixing process, the ignition, and the combustion. These instabilities cause differences in the early flame kernel development and the combustible mixture might be transported away from the spark plug or it might arrive at an unfavorable crank angle. Thus, cyclic variations effect the engine efficiency and emission of pollutants such as unburned hydrocarbons and can ultimately lead to engine misfire. Therefore, the analysis of cyclic variations via flow measurements are a major subject in the literature.

Time-resolved monoscopic PIV measurements of in-cylinder flow have been conducted by various research groups. Müller et al. [14] applied monoscopic high-speed particle-image velocimetry to the flow field of an optically accessible motored direct-injection spray-guided internal combustion engine. The flow field was sampled by 6 kHz at engine speeds of 500, 1000, and 2000 rpm. The analysis of cycle-to-cycle variations was conducted by comparing individual and cycle-averaged cycles, yielding the possibility to quantify cyclic variations using the kinetic energy. The authors discovered strong variations of the temporal evolution of the main vortex center and the kinetic energy from the mean and attributed these variations to substantially different flow regime.

Towers and Towers [18] performed monoscopic PIV flow measurements with a framing rate of 13.5 kHz at 2000 rpm

over 15 cycles for two engine conditions. The results showed a significant effect of the axial swirl level via the inlet port geometry on the cyclic variability of the flow in the latter half of the compression stroke.

Although the analysis of cyclic variations using PIV data was addressed to a great extent in the literature, no cyclic-variation studies using stereoscopic, i.e., 3C PIV, have been published so far. The goal of this study is the analysis of cyclic variations in an internal combustion using time-resolved stereoscopic PIV in the tumble plane. Mean velocity vector fields and the distribution of the mean and turbulent kinetic energy have been obtained by cycle averaging. The mean data are compared with instantaneous data from individual cycles and cyclic variations are quantified using the temporal evolution of the tumble vortex center and the kinetic energy. Furthermore, a proper orthogonal decomposition (POD) has been performed to analyze the energy distribution following Voisine et al. [20].

OPTICAL ENGINE

A four-valve DOHC single-cylinder four-stroke research engine manufactured by FEV Motorentechnik GmbH Aachen was used for the experiments. The engine offers complete optical access to the combustion chamber via a quartz glass cylinder, which imposes a low maximum allowable peak pressure. Therefore, the engine must not be fired. Instead, it is motored by a 30 kW electric engine. The engine is equipped with a tumble intake port and optimized for high tumble ratios for combustion stability in new combustion systems (compression ignition) of tailor-made fuels. Figure 1 shows the intake port geometry of the engine with a distinct "kink"-like curvature at the end of the intake port (circled area), also known as tumble port geometry. The tumble ratio of the engine is between 5 and 10, depending on the crank angle [4].

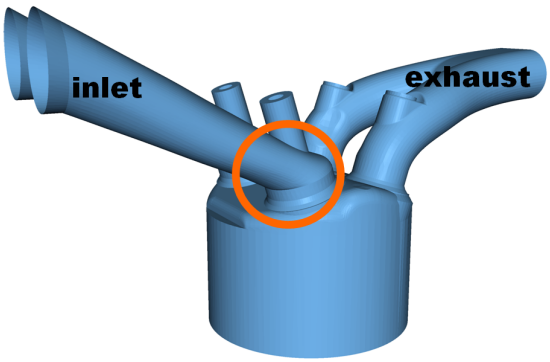

Figure 1: Tumble port geometry of the demonstrator engine.

A pronounced rotating flow is generated by this intake configuration. The engine possesses a bore of 75 mm, a stroke of 82.5 mm, and a displacement of 364 cm^3. Full optical access is achieved by a combination of a quartz glass cylinder and a quartz glass piston crown. The piston rings are located in the iron liner section and the clearance between piston and optical liner is 0.4 mm and thus sufficient to ensure a free piston movement within the optical liner. The resulting larger top-land crevice volume implies a relatively low effective compression ratio of 7.4. The engine is operated at a mean engine speed of 1,500 rpm without fuel injection and combustion. The engine is equipped with a mass balance system meeting reciprocating forces of all orders. Furthermore, a flywheel connected to the crank shaft limits the deviation of the engine speed due to compression to $\pm$ 10 rpm at an engine speed of 1500 rpm. A shaft encoder with an output of 3600 pulses per revolution and an additional pulse at top dead center (tdc) is used to measure the engine speed and the crank angle. Since the shaft encoder cannot distinct between gas exchange tdc and ignition tdc, the signal is combined with a cam shaft sensor to identify the latter. Table 1 summarizes the geometrical and operational engine parameters.

bore	75 mm
stroke	82.5 mm
displacement	364 cm^3
compression ratio	7.4
number of valves	4
exhaust valves open	110° atdc
exhaust valves close	33° atdc
inlet valves open	34° atdc
inlet valves close	250° atdc

Table 1: Engine parameters

PARTICLE-IMAGE VELOCIMETRY SYSTEM

The experimental setup for the PIV measurements is depicted in figure 2.

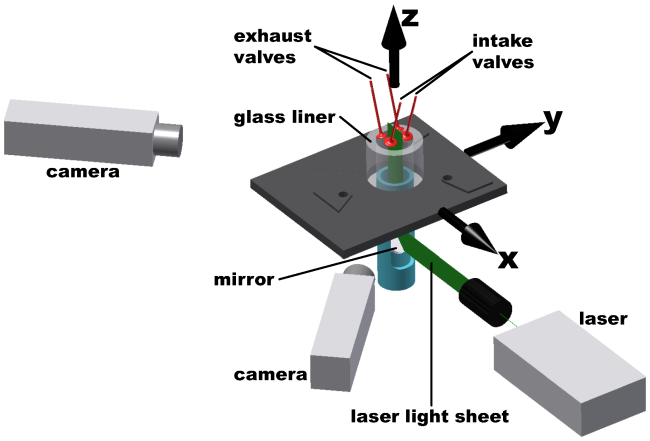

Figure 2: Experimental setup for stereoscopic PIV measurements

The PIV system consists of a pulsed Nd: YAG Laser DarwinDuo, 2 Photron SA5 double shutter PIV cameras with a resolution of 1024×1024 px^2, and two Nikon lenses with a focal length of 105 mm and a minimum f-number of 1.8. The pulse distance is 10 µs and the mapping factor is 11 px/mm. The light sheet is generated by a system of three lenses and covers the entire cylinder stroke. It has a minimum thickness of approx. 0.7 mm in the center of the field of view and a thickness of approx. 1 mm at the top and bottom. DEHS (Di-Ethyl-Hexyl-Sebacat) at a mean diameter of 0.5 µm is used as tracer particles. These particles are provided in an additional reservoir connected to the cylinder via the intake ports. Reflections on the quartz glass cylinder are widely reduced by inserting the light sheet from below through the piston crown. This setup reduces the diameter of the measuring volume to 57 mm instead of the complete bore of 75 mm, which is caused by the union nut holding the glass piston crown on top of the piston. However, Reuss et al. [17] suggest that the field of view (FOV) should be restricted to the center 66 mm of an 86 mm bore cylinder to minimize the uncertainty in detecting particle displacements. These experiments showed

that precision errors ranged between 3.5 % and 5 % of the local mean velocity. Since the FOV-to-bore ratio is almost the same in the current setup (FOV/bore = 0.76) and in the experiments conducted by Reuss et al. [17] (FOV/bore = 0.77), the errors due to cylinder curvature are minimized in the current setup.

The flow within the measurement planes is recorded at an engine speed of 1500 rpm with a sampling rate of 3.2 kHz between 25° and 345° atdc in 50 consecutive cycles for each measurement. Four measurements were performed in the symmetry plane, such that a total of 200 cycles were recorded.

PIV POST-PROCESSING

The PIV post-processing of the recorded images is done by the commercial software VidPIV (ILA GmbH, Germany). The evaluation is carried out using adaptive cross-correlation techniques with window shifting and window deformation. According to Raffel et al. [15], single exposure/double frame PIV requires a minimum particle concentration of 3 particles per interrogation window when using these techniques. Therefore, the particle concentration is set to a minimum of 3-5 particles per interrogation window for all measurement planes. The size of the interrogation windows is 32×32 px^2 with 50 % overlap. To compensate optical distortions due to the curved glass cylinder, a calibration image is taken for each individual measurement plane using an equidistant calibration grid. A velocity filter is applied which identifies a vector as an outlier if its value is more than 2.5 times the standard deviation of the median of the absolute values of the vectors in the eight surrounding interrogation windows. These outliers, i. e., in this study less than 5 %, are replaced using a second-order interpolation scheme employing the absolute values of the vectors in the eight surrounding interrogation windows.

Turbulence has a strong influence on the flame propagation speed [12] and is therefore a major factor in the analysis of the in-cylinder flow of internal combustion engines. In this study the plane averaged turbulent kinetic energy $TKE_{A,C}$ at crank angle A in cycle C:

$$TKE_{A,C} = \frac{1}{IJ}\sum_{i=1}^{I}\sum_{j=1}^{J} TKE_{A,C,i,j}, \tag{1}$$

where I and J are the number of horizontal and vertical interrogation windows, is used to define the turbulent state of the flow. The quantity $TKE_{A,C,i,j}$, i.e., the specific turbulent kinetic energy for each interrogation window, is calculated according to

$$TKE_{A,C,i,j} = \frac{1}{2}\left(u'^2_{A,C,i,j} + v'^2_{A,C,i,j} + w'^2_{A,C,i,j}\right) \tag{2}$$

where $f'_{A,C,i,j} \in \left[u'_{A,C,i,j},\, v'_{A,C,i,j},\, w'_{A,C,i,j}\right]$ is the fluctuating part of the Reynolds velocity decomposition $f_{A,C,i,j} = \bar{f}_{A,i,j} + f'_{A,C,i,j}$. The cycle-averaged velocity component $\bar{f}_{A,i,j}$ at crank angle A for each interrogation window is given by

$$\bar{f}_{A,i,j} = \frac{1}{N}\sum_{C=1}^{N} f_{A,C,i,j} \tag{3}$$

where $f_{A,C,i,j}$ corresponds to the velocity in the interrogation window $[i, j]$ at crank angle A in cycle No. C. The total number of cycles recorded is N = 200.

Furthermore, as suggested by Fajardo et al. [8], the temporal evolution of the cycle and plane averaged turbulent kinetic energy and the cycle and plane averaged mean kinetic energy will be compared to better understand the significance of the energy contained in the velocity fluctuations over time. The cycle averaged mean kinetic energy $KE_{A,i,j}$ of each interrogation window at crank angle A can be calculated according to

$$KE_{A,i,j} = \frac{1}{2}\left(\bar{u}^2_{A,i,j} + \bar{v}^2_{A,i,j} + \bar{w}^2_{A,i,j}\right) \tag{4}$$

This leads to the cycle and plane averaged mean kinetic energy KE_A at crank angle A

$$KE_A = \frac{1}{IJ}\sum_{i=1}^{I}\sum_{j=1}^{J} KE_{A,i,j} \tag{5}$$

RESULTS AND DISCUSSION

For a general overview of the flow field in the symmetry plane, Figure 3 shows the cycle-averaged velocity field in the symmetry plane between 50° and 320° atdc. The air enters the combustion chamber through the small gaps between the inlet valves and the pent roof during the intake stroke generating a counter-clockwise rotating tumble vortex that is conserved during the compression stroke. At crank angles less than 100° atdc, the flow field is dominated by the jets from the intake valves (Figure 3 a)). The inlet valves gaps cause high flow velocities and the inclination of the jets corresponds to the installation angle of the inlet valves (17.5°). At crank angles ϕ_C 100° atdc $\leq \phi_C \leq$ 150° atdc, the tumble vortex is well established and moves downwards with the piston (Figuress 3 b)-c)). Turbulence during induction is mainly generated by the free shear layer forming between the two inlet jets from the inlet valves and the in-cylinder bulk flow (Figures 3 a)-c)). During compression, the tumble moves upward with the piston (Figure 3 d)-e)) and is finally squeezed between the piston and the pent roof resulting in “tumble breakdown” [2, 3, 6]. This process describes the dissolution of the tumble vortex and and the increase in turbulence, in this case at the very top center of the combustion chamber (Figure 3 f)).

To better analyze the mechanism of tumble vortex breakdowna a proper orthogonal decomposition (POD) of the flow field in the symmetry plane is performed [20]. Figure 4 a) shows the first POD mode of the flow field at 200° atdc. This mode corresponds to the footprint of the single large tumble vortex dominating the flow in the symmetry plane. The other POD modes have more complex spatial structures, which is indicated by the illustration in figure 4 b).

Figures 5 and 6 show the temporal evolution of the first 10 POD modes for the complete engine cycle. For better visibility, the plot is decomposed into 3 and 2 subplots, respectively, and the the y-axis starts at 50 %. At early crank angles, the first POD mode captures only approx. 55 % of the total energy (Figure 5 a)). This can be attributed to the fact that at early crank angles the flow is both influenced by the downward movement of the piston and by the jets coming from the opening inlet valves. Therefore, the flow regime is very unstable and no real mean flow dominating the entire flow field has established.

The contribution of the first mode rapidly increases with increasing crank angle and the convergence, i.e., the sum of the total energy that is captured by the first ten modes, starts to increase as the piston approaches tdc (Figure 5 c)) and reaches approximately 100 % troughout the latter half of the compresion stroke (Figures 6 a)-b)). This indicates that the tumble vortex develops very early during the intake stroke and dominates the

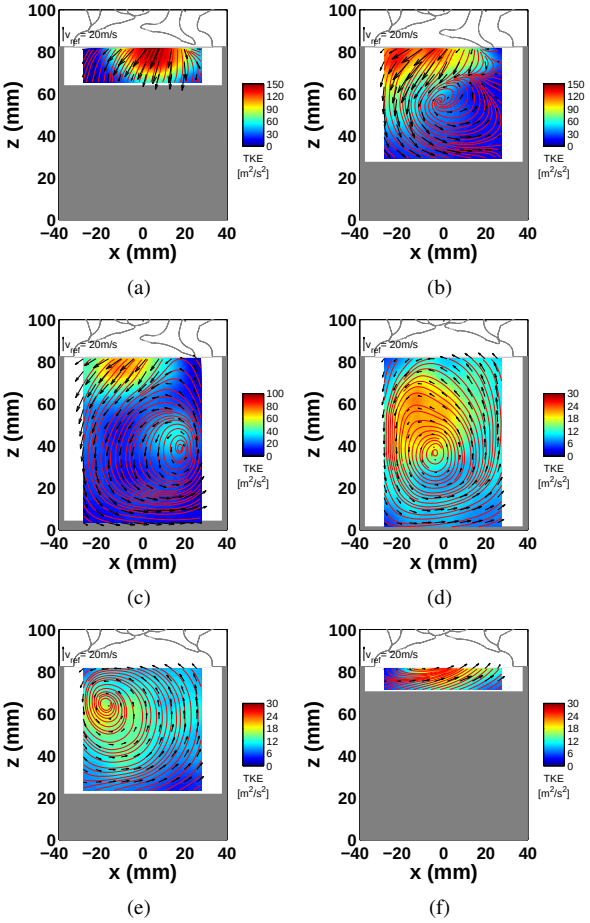

Figure 3: Cycle-averaged in-plane velocity field (black arrows), streamlines (red lines), and turbulent kinetic energy (color map) in the symmetry plane at (a) 50° atdc (b) 100° atdc, (c) 150° atdc, (d) 200° atdc, (e) 250° atdc, and (f) 320° atdc. Note, the variation of the color scaling for better visibility.

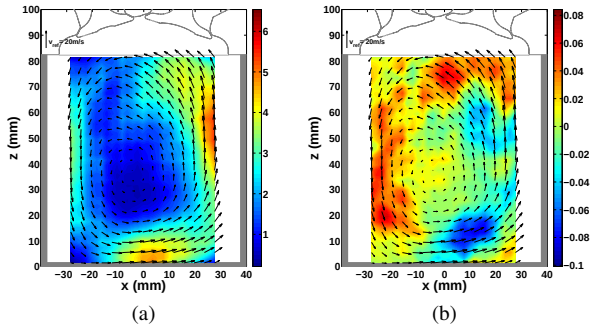

Figure 4: Cycle-averaged flow field (arrows) and contour plot of the a) first normalized POD mode and b) fourth normalized POD mode at 200° atcd in the symmetry plane

flow field. However, it is somewhat unstable during the intake stroke and stabilizes during compression. This corresponds to the observation that the turbulent kinetic energy in the vicinity of the tumble vortex is smaller in the compression stroke than in the intake stroke, see Figure 3. However, at the beginning of tumble breakdown around 320° atdc, the other POD modes rapidly increase in their contribution to the total kinetic energy of the flow such that the contribution of the first mode is again in the range of 55 %. At the same time, the convergence of the first 10 POD modes drops below 90 %. This evidences a

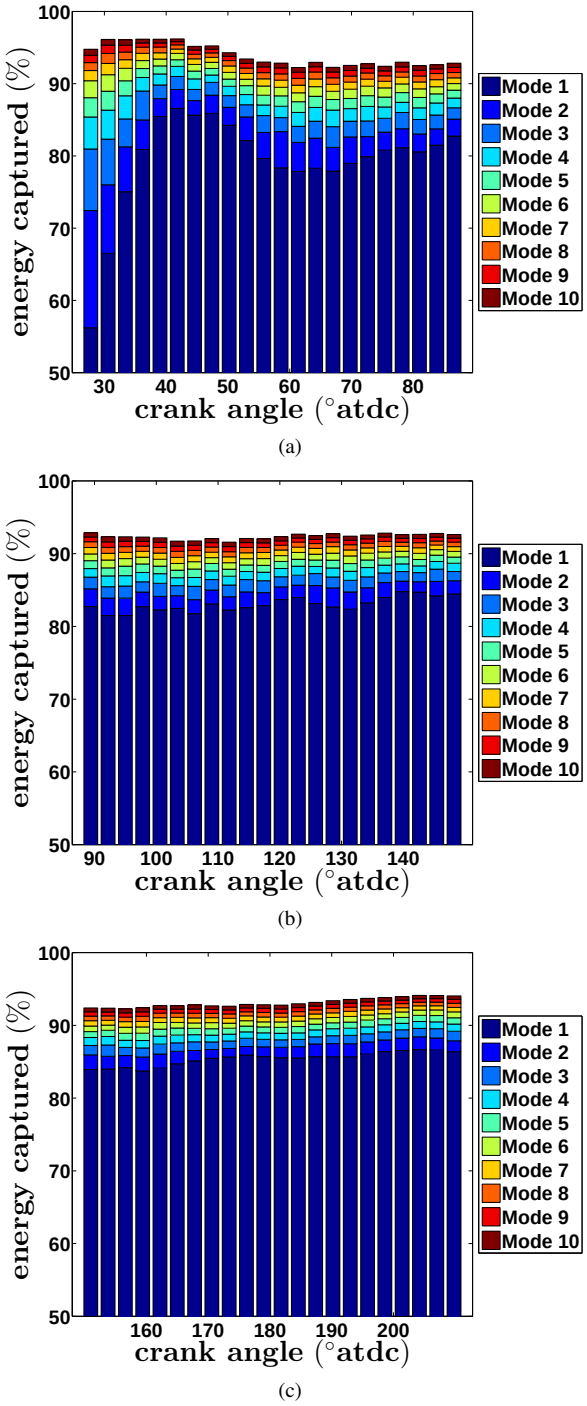

Figure 5: Temporal evolution of the first 10 POD modes between 25° atdc and 210° atdc.

transfer of energy from the lower modes to higher modes. These results agree well with the findings of Voisine et al. [20], who suggest that this transfer is both contributed to by tumble vortex breakdown and cyclic variations.

The differences of the cycle-averaged kinetic energy and the kinetic energy of a single cycle can be considered an indicator for cyclic variations [14]. Figure 7 shows the temporal development of the mean kinetic energy in the symmetry plane during induction and compression for cycles No. 10 and 20 and the distribution of the cycle-averaged mean kinetic energy.

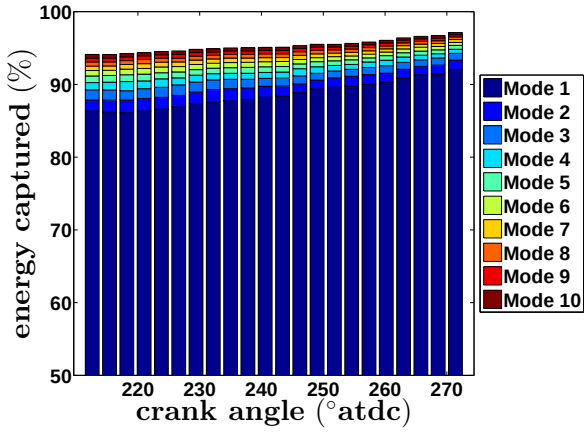

(a)

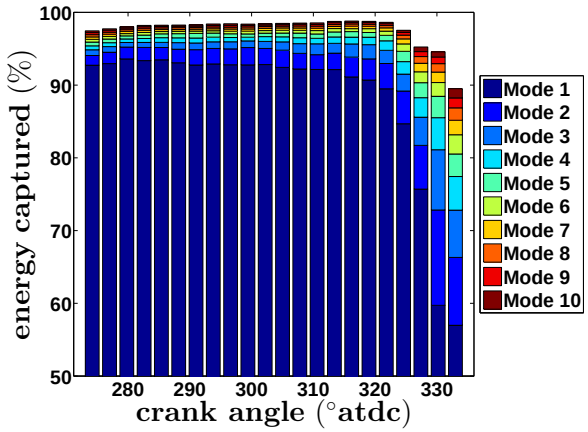

(b)

Figure 6: Temporal evolution of the first 10 POD modes between 210° atdc and 335° atdc.

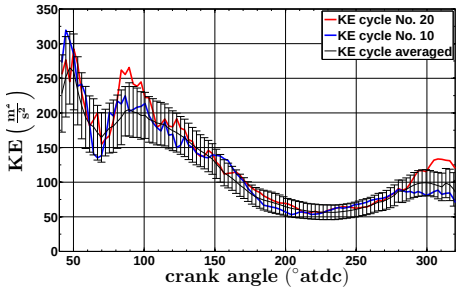

Figure 7: Temporal evolution of the mean kinetic energy in cycles No. 10 and 20 and of the cycle-averaged mean kinetic energy (error bars: standard deviation).

In general, the initially large mean kinetic energy, which is caused by the high-velocity jets of the inlet valves, decreases during intake in response to the piston motion [9] and increases again during compression. The governing flow structure in the symmetry plane is the tumble vortex, which is generated during the complete intake stroke and well conserved during compression, see Figure 3. The conservation of momentum and the decrease of volume during compression lead to the increase of the mean kinetic energy in the symmetry plane. This phenomenon is referred to as "tumble spin-up" in the literature. At the end of compression, the mean kinetic energy decreases due to tumble vortex breakdown, which is consistent with the POD analysis.

The comparison of the temporal development of the mean kinetic energy in cycles No. 10 and 20 shows that in certain individual cycles the mean kinetic energy is well within the standard deviation such as the No. 10 distribution. In other individual cycles, however, the mean kinetic energies shows some discrepancies and temporally extends the bandwith of the standard deviation. For example, in cycle No. 20 the mean kinetic energy around 90° atdc is above the standard deviation. This is an indicator for a higher mean flow velocity which might be caused by a low in-cylinder pressure in this cycle. At the end of compression in cycle No. 20, the kinetic energy keeps rising although the mean has already started to decrease due to tumble breakdown. This indicates that the tumble breakdown takes place at later crank angles in cycle No. 20, which is again an indicator for a cyclically perturbed flow structure.

The comparison of the temporal development of the turbulent kinetic energy in individual cycles and the cycle average is another indicator for cyclic variations [14]. Figure 8 shows the temporal development of the turbulent kinetic energy in the symmetry plane during induction and compression for cycles No. 11 and 26, respectively, and of the cycle-averaged turbulent kinetic energy.

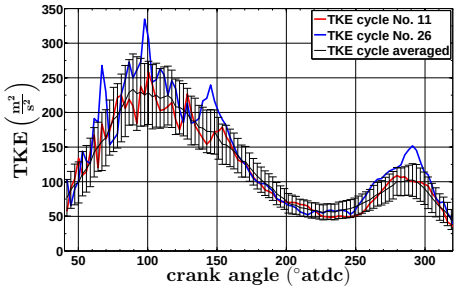

Figure 8: Temporal evolution of the turbulent kinetic energy in cycles No. 11 and 26, and of the cycle-averaged turbulent kinetic energy (error bars: standard deviation).

In general, the turbulent kinetic energy increases during the intake stroke and reaches its maximum around 90° atdc. This increase is due to the turbulence production in the free shear layers that form between the jets from the intake valves and the bulk flow in the combustion chamber, see Figure 3. During the latter half of induction and the first half of compression, the turbulent kinetic energy decreases. This is due to a decrease of turbulence production and enhanced dissipation due to viscous shear stress [9]. Towards the end of compression, the turbulent kinetic energy increases due to the beginning breakdown of the tumble vortex. Like in the findings of the distribution of the mean kinetic energy in Figure 7, there are individual cycles where the turbulent kinetic energy is well within the standard deviation, e.g. cycle No. 11. In other individual cycles, however, the turbulent kinetic energy shows significant discrepancies in comparison to the cycle average and lies outside the standard deviation. For example, in cycle No. 26, the turbulent kinetic energy during the intake phase is above the standard deviation. This can be attributed to a higher rate of turbulence production due to the free shear layers between the inlet jets and the combustion chamber bulk flow. At the end of compression in cycle No. 26, the turbulent kinetic energy is again well above the standard deviation. This can be attributed to an earlier tumble breakdown in this cycle.

Next, following the analysis of Bücker et al. [3], the path of the tumble vortex core in individual cycles with the cycle-averaged path is investigated. Figure 9 shows the cycle averaged velocity field at 180° atdc (a), the value of the cycle averaged

Γ_1-criterion [10] at 180° atdc (b), and the cycle averaged path of the tumble vortex core during intake and compression (a) and b)). The clockwise movement of the tumble core is clearly visible. Note that there seems to be a "jump" of the vortex core around halfway during compression. This does not correspond to a physical displacement of the tumble vortex core. As a matter of fact, at approx. 200° atdc, the tumble vortex starts to merge with two ring vortices that develop beneath the inlet valves. The Γ_1-criterion detects the single merged vortex that remains at later crank angles rather than the "original" tumble vortex. For a detailed description of this phenomenon, see [3].

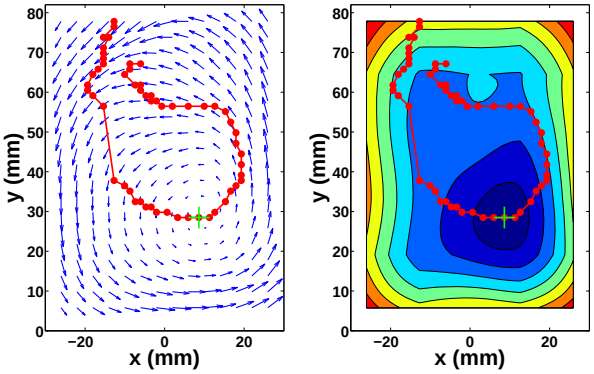

Figure 9: a) Cycle-averaged velocity field at 180° atdc (arrows), path of the tumble vortex core during intake and compression (red line), and position of the tumble vortex core at 180° (green cross) in the symmetry plane. b) Γ_1 contours (contour plot), path of the tumble vortex core during intake and compression (red line), and position of the tumble vortex core at 180° (green cross) in the symmetry plane.

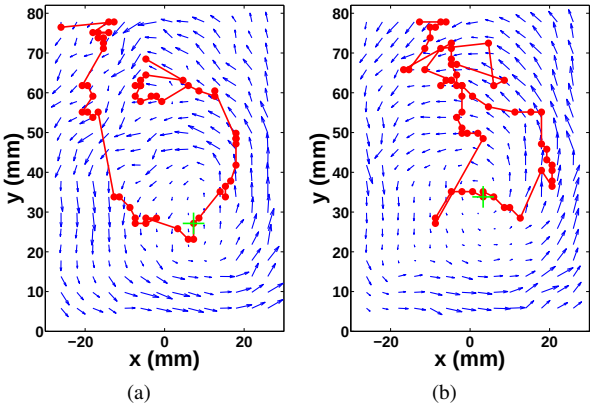

Figure 10: a) Instantaneous velocity field at 180° atdc (blue arrows), path of the tumble vortex core during intake and compression (red line), and position of the tumble vortex core at 180° (green cross) in the symmetry plane in cycle No. 43. b) Instantaneous velocity field at 180° atdc (blue arrows), path of the tumble vortex core during intake and compression (red line), and position of the tumble vortex core at 180° (green cross) in the symmetry plane in cycle No. 33.

Figure 10 shows the velocity field at 180° atdc and the path of the tumble vortex core in cycles No. 33 and 43. In cycle No. 43, the path of the tumble vortex core is similar to the cycle-averaged path. The downward movement on the right-hand side, the lateral movement around bdc, and the upward movement on the left-hand side are very similar to the cycle averaged case. Note that the "jump" takes place at the same crank angle in the cycle-averaged path and in the path of cycle No. 43. In cycle No. 33, however, the picture is extremely different. While the downward movement on the right-hand side during intake is similar to the cycle averaged path and there is also a lateral movement around bdc, the path differs significantly during the compression stroke. The tumble vortex core moves upward through the center of the combustion chamber rather than on the left hand side. The "jump" takes place at a much earlier crank angle and finally, the path intersects with itself at the end of combustion and the beginning of induction. This clearly shows the different flow structure in this cycle.

CONCLUSION AND OUTLOOK

The highly unsteady three-dimensional flow structures during the intake and the compression stroke of an optical four-stroke four-valve single-cylinder gasoline type demonstrator engine are analyzed using time-resolved stereoscopic particle-image velocimetry (PIV). The flow is measured in the tumble plane, the main vortical structure is visualized, i.e., the main tumble in the symmetry plane between the inlet and outlet valves, and the temporal development of the turbulent kinetic energy is determined.

The analysis of the flow field shows that the tumble vortex is the major player in the flow field throughout intake and compression and that it breaks down at approx. 320° atdc. The POD analysis shows that the tumble vortex forms at early crank angles, dominates the flow regime, and stabilizes during the compression stroke. With the beginning of the tumble breakdown, the first POD mode drops rapidly, indicating an energy transfer to higher modes which might be caused by both tumble vortex breakdown and cyclic variations.

The analysis of the temporal development of the mean kinetic energy shows that in individual cycles the mean kinetic energy is well within the standard deviation. In other individual cycles, however, the mean kinetic energy shows significant discrepancies. These discrepancies indicate higher mean flow velocities during induction, probably caused by a lower in-cylinder pressure, and a later tumble breakdown, evidenced by a stronger increase of the mean kinetic energy towards the end of combustion. Discrepancies are also observed in the temporal development of the turbulent kinetic energy. In individual cycles, the turbulent kinetic energy during the intake phase is above the standard deviation of the cycle mean, indicating a higher rate of turbulence production due to the free shear layers between the inlet jets and the combustion chamber bulk flow. At the end of compression, higher turbulent kinetic energy can also be observed, indicating an earlier tumble breakdown cycle in this cycle. Finally, the differences in individual paths of the tumble vortex core are a strong indicator that significant cyclic variations do occur in the demonstrator engine.

The analysis focuses on the three-component velocity field in the symmetry plane of the in-cylinder flow, since the main flow structure, i.e., the tumble vortex is present in this plane. However, the flow field in internal combustion engines is of highly three-dimensional nature. Therefore, as a next step, it is intended to investigate the in-cylinder flow field in multiple planes with time resolved stereoscopic PIV. Furthermore, time resolved tomographic PIV is to be used to analyze the flow field.

REFERENCES

[1] C. Arcoumanis, J. H. Whitelaw, “Fluid mechanics of internal combustion engines - a review”, Proceedings of the Institution of Mechanical Engineers, Vol. 201 No. 1, pp. 57-74, 1987.

[2] J. Boree, S. Maurel, R. Bazile, “Disruption of a compressed vortex”, Physics of Fluids, Vol. 14 No. 7, pp. 2543-2556, 2002.

[3] I. Bücker, D.-C. Karhoff, M. Klaas, and W. Schröder, “Stereoscopic multi-planar PIV measurements of in-cylinder tumbling flow”, Experiments in Fluids, Vol. 53 No. 6, pp. 1993-2009, 2012

[4] I. Bücker, D. Karhoff, J. Dannemann, K. Pielhop, M. Klaas, W. Schröder, “Comparison of PIV Measured Flow Structures in Two Four-Valve Piston Engines”, New Results in Numerical and Experimental Fluid Mechanics VIII: Contributions to the 17th STAB/DGLR Symposium Berlin, Germany, 2010 Notes on Numerical Fluid Mechanics and Multidisciplinary Design, Vol. 121, Springer, Berlin, pp. 633-640, 2013.

[5] P. O. Calendini, T. D. A. Lecerf, M. Trinite, “In-cylinder velocity measurements with stereoscopic particle image velocimetry in a SI engine”, SAE 2000-01-1798, 2000.

[6] J. Dannemann, K. Pielhop, M. Klaas, W. Schröder, “Cycle resolved multi-planar flow measurements in a four-valve combustion engine”, Experiments in Fluids, Vol. 50 No. 4, pp. 961-976, 2011.

[7] P. Druault, P. Guibert, F. Alizon, “Use of proper orthogonal decomposition for time interpolation from PIV data”, Experiments in Fluids Vol. 39 No. 6, pp 1009-1023, 2005.

[8] C. Fajardo, V. Sick, “Development of a high-speed UV particle image velocimetry technique and application for measurements in internal combustion engines”, Experiments in Fluids, Vol. 46 No. 9, pp. 43-53, 2009.

[9] S. Fiveland, and D. Assanis, “A Four-Stroke Homogeneous Charge Compression Ignition Engine Simulation for Combustion and Performance Studies”, SAE Technical Paper 2000-01-0332, 2000.

[10] L. Graftieaux, M. Michard, N. Grosjean, “Combining PIV, POD and vortex identification algorithms for the study of unsteady turbulent swirling flows” Measurement Science and Technology, Vol. 12, pp. 1422-1429, 2001

[11] J.B. Heywood, “Fluid motion within the cylinder of internal combustion engines”, J. Fluids Eng. Vol. 109 No. 1, pp. 3-35, 1987.

[12] J. B. Heywood, “Internal Combustion Engine Fundamentals”, McGraw-Hill, New York, ISBN 007028637X, 1988.

[13] R. F. Huang, K. H. Lin, C.-N. Yeh, J. Lan, “In-cylinder tumble flows and performance of a motorcycle engine with circular and elliptic intake ports”, Experiments in Fluids Vol. 46 No. 1, pp. 165-179, 2009.

[14] S. H. R. Müller, B. Böhm, M. Gleißner, R. Grzeszik, S. Arndt, A. Dreizler“, Flow field measurements in an optically accessible, direct-injection spray-guided internal combustion engine using high-speed PIV”, Experiments in Fluids, Vol. 48 No. 2, pp. 281-290, 2010.

[15] M. Raffel, C. Willert, S. Wereley, J. Kompenhans, “Particle Image Velocimetry: A Practical Guide”, Springer, Berlin, ISBN 3540723072, 2007.

[16] D. Reuss, R. Adrian, C. Landreth, D. French, T. Fansler, “Instantaneous planar measurements of velocity and large-scale vorticity and strain rate in an engine using particle image velocimetry” SAE paper 890616, 1989.

[17] D. L. Reuss, M. Megerle, V. Sick, “Particle-image velocimetry measurement errors when imaging through a transparent engine cylinder”, Measurements Science and Technology, Vol. 13 No. 7, pp. 1029-1035, 2002.

[18] D. P. Towers and C. E. Towers, “Cyclic variability measurements of in-cylinder engine flows using high-speed particle image velocimetry”, Measurement Science and Technology, Vol. 15 No. 9, pp. 1917-1925, 2004.

[19] K. Stapf, D. Seebach, F. Fricke, S. Pischinger, K. Hoffmann, D. Abel, “CAI-Engines: modern combustion system to face future challenges”, SIA Int. Conference-The Spark Ignition Engine of the Future, France, December 2-3, 2009.

[20] M. Voisine, L. Thomas, J. Boree, P. Rey, “Spatio-temporal structure and cycle to cycle variations of an in-cylinder tumbling flow”, Experiments in Fluids, Vol. 50 No. 5, pp. 1393-1407, 2011.

ACKNOWLEDGMENTS

This research was performed as part of the Cluster of Excellence “Tailor-Made Fuels from Biomass” which is funded by the German Excellence by the German federal and state governments to promote science and research at German universities. Furthermore, the financial support by the DFG by the NRW Forschungsschule “Brennstoffgewinnung aus nachwachsenden Rohstoffen (BrenaRo)”is gratefully acknowledged.